

Ultrafast relaxation of highly excited hot electrons in Si: Roles of the L – X intervalley scattering

T. Ichibayashi, S. Tanaka, J. Kanasaki, and K. Tanimura*

The Institute of Scientific and Industrial Research, Osaka University, 8-1 Mihogaoka, Ibaraki, Osaka 567-0047, Japan

Thomas Fauster

Lehrstuhl für Festkörperphysik, Universität Erlangen-Nürnberg, Staudtstrasse 7, Bau A3, D-91058 Erlangen, Germany

(Received 2 April 2011; revised manuscript received 29 September 2011; published 27 December 2011)

Two-photon photoemission (2PPE) spectroscopy is used to reveal dynamic relaxation of highly excited electrons generated by 3 eV photons in Si. Monochromatic 2PPE at probe-photon energies ranging from 3.2 to 3.5 eV reveals a coherent 2PPE peak from the valence band maximum, and a transiently populated photoemission peak near L_1 in the conduction band. Time-resolved 2PPE measurements show that electrons injected into the L valley undergo L-to-X intervalley scattering with a time constant of 180 fs at 293 K. A deformation potential constant of $1.2 \text{ eV}\text{\AA}^{-1}$ is obtained for the scattering. The highly excited electrons are relaxed down around the conduction band minimum to form a quasi-equilibrated hot electron distribution; the highest density is accumulated at 660 fs after excitation. The hot electron distribution is equilibrated with the lattice within 2 ps after excitation. These results are compared to relaxation processes of electrons injected directly into the X valley by photons with energies below 2.2 eV.

DOI: [10.1103/PhysRevB.84.235210](https://doi.org/10.1103/PhysRevB.84.235210)

PACS number(s): 78.47.J–, 73.20.At, 78.55.Ap, 79.60.Bm

I. INTRODUCTION

Ultrafast semiconductor carrier dynamics are of great scientific and technological interest. Many of the dynamics in short temporal domains are defined by electron-phonon interaction, together with carrier-carrier interactions; phonon-induced scattering processes transfer carriers between different momentum states and finally thermalize hot carriers with the lattice. Despite the importance of Si to fundamental semiconductor physics and the microelectronics industry, most knowledge of electron-phonon interactions is limited to near-equilibrium conditions and obtained by transport measurements. Recently, a greater understanding of the interactions in Si has become increasingly important. First, in nanoscale devices with dimensions comparable to carrier scattering lengths, fundamental quantum-mechanical carrier-lattice interactions determine their properties.¹ Therefore, a comprehensive understanding of electron-phonon interaction over the full Brillouin zone is important. Second, photoexcitation of Si at photon energies of more than 3 eV induces striking structural rearrangements in Si, such as coherent phonon excitations,² electronic surface bond rupture,³ and electronically driven order-disorder phase transitions.⁴ For a mechanistic understanding of these phenomena, a comprehensive study of the ultrafast carrier dynamics in Si at wider momentum and energy ranges is crucial.

Extensive theoretical and experimental studies have fully characterized the Si electronic structure.^{5–12} In Fig. 1, we show the band structure of Si along the L- Γ -X directions of the Brillouin zone⁵ and the transition pathways concerned in this paper schematically. Several optical spectroscopic studies have shown that direct transitions E'_0 at the zone center and E_1 at near the L critical point occur at $3.31 \pm 0.03 \text{ eV}$ and $3.39 \pm 0.02 \text{ eV}$ at 296 K, respectively. Since the energy of L_1 at the conduction band (CB) is 2.2 eV above the valence band maximum (VBM),⁵ hot electrons generated by excitation with photon energies smaller than 2.2 eV are injected directly into the states along the Γ -X line, and they are relaxed down

near the conduction band minimum (CBM) via intravalley scattering. The ultrafast dynamics of intravalley scattering of hot electrons have been studied using femtosecond (fs)-laser excitation to show some characteristic features of the relaxation scattering.¹³ At higher photon energies, but still below the direct transitions, a significantly increasing absorption coefficient¹⁴ has been attributed to indirect transitions into the L and/or X valleys. For such highly excited electrons, intervalley scattering among L, Γ , and X valleys in the CB, associated with large momentum transfer, becomes important in ultrafast carrier relaxation. In order to trace the relaxation pathways for these hot electrons precisely, dynamical studies of momentum- and energy-resolved states are needed.

Optical techniques used to study ultrafast carrier relaxation in Si have been restricted mainly to measurements of transient changes in the dielectric function following excitation by laser pulses. The indirect band gap of Si precludes more specific probes, such as time-resolved luminescence measurements, which are often applied to direct band-gap compound semiconductors.¹⁵ More importantly, the final states of optical transitions cannot be traced using an optical technique; knowledge of carrier relaxation in momentum space may only be inferred indirectly. On the other hand, photoemission spectroscopy measures the energy and parallel momentum. Two-photon photoemission spectroscopy (2PPE), including time- and angle-resolved measurements, provides a direct spectroscopic technique to determine the final states of optical transitions, and energy- and momentum-resolved dynamics.¹⁶

In this paper, we present a 2PPE study of the dynamic relaxation of highly excited hot electrons in Si using photon energies from 3.2 to 3.5 eV. Monochromatic 2PPE at probe-photon energy ($h\nu_{\text{pr}}$) in this range reveals a coherent 2PPE peak from the VBM, and a photoemission peak from transiently populated electrons at the L valley in the CB. Time-resolved 2PPE measurements show that electrons injected into the L valley undergo L-to-X intervalley scattering with a time constant of 180 fs at 293 K. A deformation potential constant

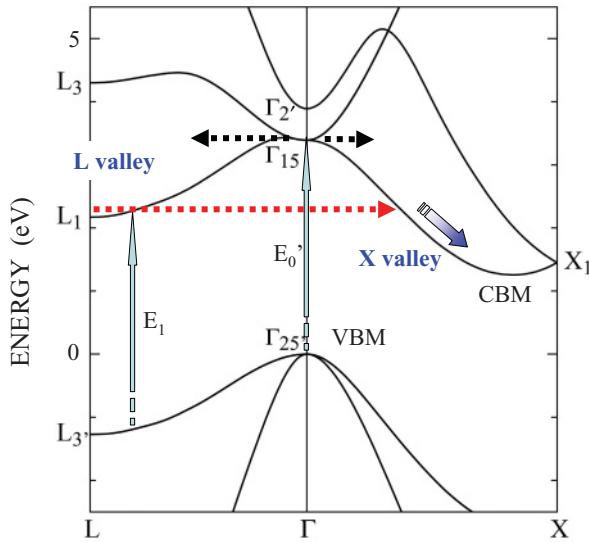


FIG. 1. (Color online) Band structure of Si along L- Γ -X (from Ref. 5), and transition pathways discussed in this paper. The energy is referenced with the valence band maximum.

of $1.2 \text{ eV}\text{\AA}^{-1}$ is obtained for the scattering. The relaxation of highly excited electrons leads to the formation of a quasi-equilibrated hot electron distribution around the CBM, and the highest density is accumulated near the CBM at 660 fs after excitation. The hot electron distribution is equilibrated with the lattice within 2 ps after excitation. These results are compared to relaxation processes of electrons injected directly into the X valley by excitation at 2.10 eV, in order to highlight characteristic features of relaxation of hot electrons generated by 3 eV photons.

II. EXPERIMENTAL METHODS

Boron-doped *p*-type Si(001) and Si(111) wafers with resistivity of 4.8 and $5.1 \Omega\cdot\text{cm}$ were clamped with Ta sheets to the sample holder in an ultrahigh-vacuum chamber ($<5 \times 10^{-11}$ Torr). Surface structures were characterized *in situ* by a scanning tunneling microscope prior to photoemission measurements. The (100) surfaces were well-ordered double-domain (2×1) structures with a typical surface-defect concentration n_D of 1%, while (111) surfaces were almost perfect (7×7) structures with n_D less than 0.05%. A 76 MHz Ti-sapphire laser was used to generate fs-laser pulses from 700 to 765 nm. The second (2ω) and third (3ω) harmonics of the fundamental (ω) were used in the 2PPE experiments. The fundamental was used to establish the flat-band conditions for the Si(111)- (7×7) surface, where band bending is significant.^{17–19} The fundamental laser pulses hit the surfaces about 10 ns before the photoemitting pulses. The temporal width of the ω and 2ω pulses was typically 100 fs, but the width of 3ω pulses was broadened to 180 fs due to optical dispersion of a pair of lenses and the window of the ultrahigh-vacuum chamber. We also used a femtosecond laser system consisting of a regenerative amplifier of the Ti:Sapphire laser and optical parametric amplifier, which generates 120 fs laser pulses centered at a photon energy of 2.10 eV. A part of the amplified fundamental output at 765 nm was used to generate

third harmonics to probe photoemission. The temporal width was 160 fs at the sample position. The pump and probe pulses, with a preset time delay (Δt), were aligned coaxially and focused on the sample surfaces at 45° to normal. Electrons emitted along the surface normal ($\pm 2^\circ$) were analyzed using a hemispherical analyzer with an instrumental energy resolution of 50 meV.

For Si(111)- (7×7) , electron populations along the Γ - Δ -L line in the CB can be monitored by measuring surface-normal photoemission. Also, the population near the CBM can be detected simultaneously because of the reduced surface Brillouin zone for this surface.²⁰ For Si(001)- (2×1) , surface-normal photoemission probes the states not only along the Γ - Δ -X line but along $2/3\Sigma$ -L, due to back folding to $\bar{\Gamma}$ by the 2×1 reconstruction for Si(001)- (2×1) .²¹ Therefore, use of the two different surfaces makes it possible to characterize the relaxation pathways of highly excited electrons in Si in wider momentum spaces, and to examine the effects of surface states on carrier dynamics in bulk electronic states of Si.

III. RESULTS AND DISCUSSION

A. Energy-resolved 2PPE

1. Monochromatic 2PPE with 2ω pulses

Figure 2(a) shows the monochromatic 2PPE spectra measured by *p*-polarized probe light with $h\nu_{\text{pr}}$ from 3.24 to 3.44 eV for Si(111)- (7×7) at 293 K. The electron energy E for the spectra is given with reference to the vacuum

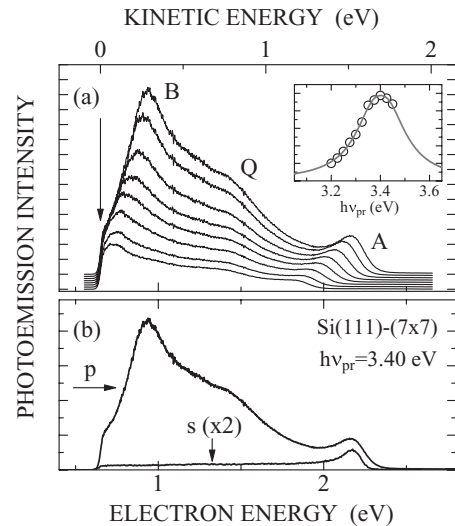


FIG. 2. (a) Two-photon photoemission spectra from Si(111)- (7×7) measured for *p*-polarized probe pulses with $h\nu_{\text{pr}}$ from 3.24 to 3.40 eV at 293 K. The $h\nu_{\text{pr}}$ are 3.24, 3.26, 3.28, 3.30, 3.33, 3.35, 3.37, and 3.40 eV from the bottom to the top. Three peak features in the spectra are labeled as A, B, and Q. The inset shows the intensity of peak A as a function of $h\nu_{\text{pr}}$. (b) Comparison of two-photon photoemission spectra measured for *p*- and *s*-polarized probe pulses at $h\nu_{\text{pr}} = 3.40$ eV at 293 K. The intensity of *s*-polarized spectrum is multiplied by a factor of 2. In both (a) and (b), the energy is referenced to the work function of the analyzer at the bottom scale, while it is converted to the kinetic energy referenced to the vacuum level of specimens at the upper scale.

level of the analyzer. The intensities of the spectra measured at different $h\nu_{\text{pr}}$ values are normalized with respect to the square of the photon flux (number of photons per unit area). The normalization evidences just the photoemission resonance enhancement and does not change any spectral features. In the figure, we clearly see two peaks, labeled as A and B, and a shoulder-like structure labeled as Q. In the inset of the figure, we show the peak intensity of the highest-energy peak A as a function of $h\nu_{\text{pr}}$. It shows a resonance enhancement at $h\nu_{\text{pr}} = 3.40$ eV. The intensity of peak B increases with increasing $h\nu_{\text{pr}}$ up to the highest $h\nu_{\text{pr}}$ used in this study.

In Fig. 2(b), we compare the 2PPE spectra measured by *s*- and *p*-polarized probe light at $h\nu_{\text{pr}} = 3.40$ eV. In the spectrum measured by *p*-polarized light, the energies of peaks A and B are 2.17 and 0.94 eV, respectively, and peak Q is located at around 1.5 eV. On the other hand, although the highest energy peak A can be excited, peaks B and Q are almost completely suppressed for *s*-polarized light. The probe-light polarization dependence gives important information about the symmetries of the initial and intermediate states involved in the 2PPE processes.

In the spectra shown in Fig. 2, there is a clear and common low-energy cutoff E_L , which corresponds to the difference between the vacuum level Φ_v of Si(111)-(7 × 7) surfaces used in the measurement and the vacuum level of the electron analyzer, both of which are connected by a common Fermi level E_F . It is well known that surface band bending exists on this surface, and the surface photovoltaic effect is significant when the surface is photoexcited.^{17–19} The surface Fermi level measured from the VBM is not the same as E_F in the bulk in such cases. Since the work function (4.337 eV) of the analyzer, E_F (0.24 eV above VBM) in the bulk of our specimens, and the ionization energy χ (5.31 eV) of Si(111)-(7 × 7) are known,^{20,22,23} E_L for the surface under complete flat-band conditions can be estimated to be 0.73 eV. The observed E_L in Fig. 2 is 0.65 eV, about 0.1 eV less than that expected for flat-band conditions, showing that a finite amount of band bending still exists for our experimental conditions at 293 K. Keeping this fact in mind, we change the energy axis from the electron energy, referenced by the vacuum level of the analyzer, to the kinetic energy E_K , defined as $E_K = E - E_L$. The upper scale of Fig. 2 shows the kinetic energy using $E_L = 0.65$ eV. Since all states in the surface region monitored by 2PPE shift their energies in parallel,¹⁷ use of E_K gives a more reliable energy axis to analyze the spectra in terms of electronic states of Si by compensating for possible variations of photovoltage coming from different excitation and/or probe conditions. In reality, however, an E_L value of 0.65 eV is rather insensitive to different excitation/probe conditions, as seen in Fig. 2, and varies at most by ± 0.02 eV when the fundamental of fs-laser light is used to reduce band bending. The photovoltaic effects and several consequences of laser-induced removal of band bending will be fully described in a separate paper.²⁴

The shifts in the peak kinetic energy E_{KP} as a function of $h\nu_{\text{pr}}$ give crucial information to identify the photoemission processes of 2PPE.^{21,25} In order to compare the results of monochromatic 2PPE using 2ω pulses with those obtained by bichromatic 2PPE using 2ω and 3ω pulses as described later, we analyze the peak-energy shifts of photoemission peaks in Fig. 2(a) in terms of the photon energy ($h\nu_0$) of the fundamental

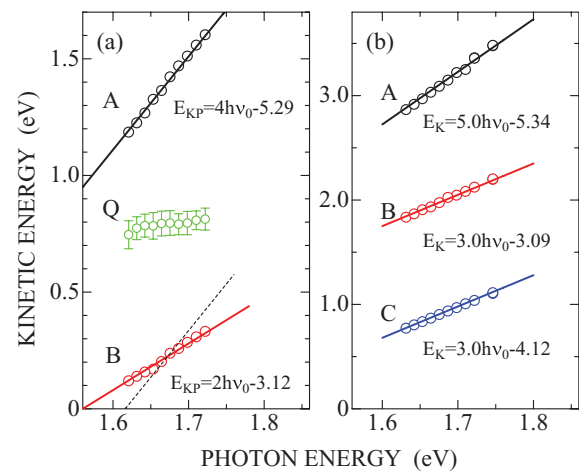


FIG. 3. (Color online) (a) The peak kinetic energy E_{KP} of peaks A, B, and Q in Fig. 2(a) as a function of photon energy ($h\nu_0$) of the fundamental of the second harmonics used for probe light. The dashed line with slope = 4 is shown for comparison also for peak B. (b) The peak kinetic energy of peaks A, B, and C in Fig. 5, obtained by bichromatic two-photon photoemission measurements with 2ω and 3ω pulses as a function of photon energy of the fundamental of 2ω and 3ω light pulses.

of fs-laser light; $h\nu_{\text{pr}} = 2 h\nu_0$. In this case, E_{KP} can be expressed as $E_{KP} = mh\nu_0 - E_i$, where m is a constant, and E_i is the energy of the initial state of photoemission measured from Φ_v . For a peak due to a coherent 2PPE process from an occupied state, the energy of the state is given by E_i , and $m = 4$ is expected. On the other hand, when a photoemission peak is due to an incoherent two-step process, the initial state is a normally unoccupied state, which is transiently occupied within a pulse, and m takes the value of 2.²⁵ As seen in Fig. 2(a), peaks A and B show sizable peak-energy shifts with increasing $h\nu_{\text{pr}}$, while peak Q shows almost no shift. Also, its shoulder-like structure makes it difficult to determine the peak kinetic energy precisely. Therefore, we omit peak Q in this analysis.

In Fig. 3(a), E_{KP} of each peak is plotted as a function of $h\nu_0$. Peak A shows $m = 4$ and $E_i = 5.29$ eV below Φ_v , while peak B shows $m = 2$ and $E_i = 3.12$ eV below Φ_v . The broken curve with a slope of 4 is added to emphasize the character of $m = 2$ for peak B. The result of $m = 4$ for peak A is a clear indication that the peak is due to coherent 2PPE by a 2ω laser pulse from an occupied state with a constant energy. On the other hand, the value $m = 2$ for peak B is strongly suggestive that the peak comes from a two-step photoemission process, including transient population of a normally unoccupied state followed by one-photon photoionization within a laser pulse.

In Fig. 4, we show the monochromatic 2PPE spectra measured for surface-normal photoemission from Si(001)-(2 × 1) surfaces at 293 K, using $h\nu_{\text{pr}}$ from 3.33 to 3.44 eV. The energy scale in the figure is the kinetic energy introduced previously. In the figure, a three-peak structure, similar to that for Si(111)-(7 × 7), is clearly detected, although the lowest energy peak, labeled B', is reduced strongly in intensity relative to the highest-energy peak, labeled A', for Si(001), when we compare the spectral features for the two surfaces. When *s*-polarized 2ω light is used, peak A' is excited, while peaks B'

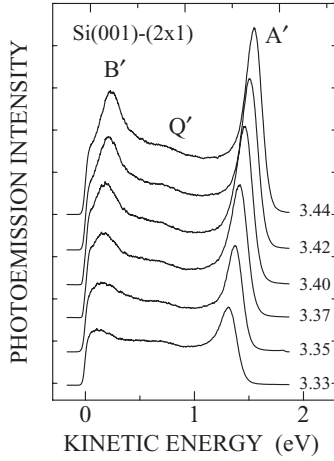


FIG. 4. Two-photon photoemission spectra from Si(001)-(2 × 1) measured for *p*-polarized probe pulses at $h\nu_{pr}$ from 3.33 to 3.44 eV at 293 K. Three peaks in the spectra are labeled as A', B', and Q', respectively. The energy is referenced to the vacuum level of the surface, giving the kinetic energy of photoelectrons.

and Q' are almost completely suppressed, similar to the case of Si(111)-(7 × 7). We analyzed the shifts of peaks A' and B' in Fig. 4 in terms of the photon energy ($h\nu_0$) of the fundamental of fs-laser light, similar to the case of Si(111)-(7 × 7). It is found that peak kinetic energy $E_{KA'}$ for peak A' is described as $E_{KA'} = 4h\nu_0 - 5.34\text{eV}$, and that the energy $E_{KB'}$ for peak B' is given as $E_{KB'} = 2h\nu_0 - 3.21\text{eV}$. Based on these results, we can conclude that peak A' is due to a coherent 2PPE process, and peak B' is a two-step photoemission from a transiently populated normally unoccupied state. As seen in Fig. 4, peak Q' shows almost no changes in peak energy with changing $h\nu_{pr}$, similar to the case of peak Q of Si(111)-(7 × 7), suggesting a similar origin for the two peaks.

In order to compare the two photoemission peaks observed for two different surfaces, we have to take the different ionization energies into account. The χ of 5.35 ± 0.05 eV has been reported for Si(001).^{21,22,26,27} The magnitudes of E_i values determined here are listed in Table I, together with χ values reported in literature. Because of the scatter of ionization energies reported, the energies of the initial states with respect to the VBM can be determined within uncertainties of ± 0.05 eV. Within this limitation, we can conclude that the initial state of peak A of the Si(111) surface and that of peak A' of the Si(001) surface have the same energy relative to the VBM. The estimated energy of the initial state is the same as the VBM within experimental error. Also, we find that the initial state of peak B of the (111) surface and that of peak B' of the (001) surface, both of which are due to incoherent two-step photoemission processes, are the same, and located about 2.1 eV above the VBM. We discuss the initial states of the photoemission processes in detail after adding some more information from bichromatic 2PPE results in the next section.

2. Bichromatic 2PPE with 2 ω and 3 ω pulses

In order to elucidate the 2PPE processes further, we used 2 ω and 3 ω pulses to measure bichromatic 2PPE spectra from Si(111)-(7 × 7). In the study of time-resolved 2PPE to

TABLE I. Initial-state energy (E_i) determined by the analysis using $E_{KP} = m h \nu_0 - E_i$ for each photoemission peak detected in monochromatic 2PPE measurements for Si(111)-(7 × 7) and Si(001)-(2 × 1). A simple average value is taken for the ionization energy (χ) for each surface over reported values in the literature. Energy (E_V) relative to the VBM is estimated from E_i and ξ . The constant m used in the analysis is in the last column.

Surface	χ (eV)	Peak	E_i (eV)	E_V (eV)	m
(111)	5.31 ± 0.04^a	A	-5.29	0.02 ± 0.04	4
		Q	-	-	~ 0.5
		B	-3.12	2.19 ± 0.04	2
(001)	5.35 ± 0.05^b	A'	-5.34	0.01 ± 0.05	4
		Q'	-	-	~ 0.8
		B'	-3.21	2.14 ± 0.05	2

^aReferences 20, 22, and 23.

^bReferences 21, 22, 26, and 27.

reveal dynamics of photogenerated highly excited electrons, introduction of 3 ω pulses as probe pulses extends our energy window by more than 1.5 eV, which is essential for detecting transient electron populations in a wider energy range that includes the CBM. As shown in our previous study, the CBM photoemission is observed only for *p*-polarized probe light, mainly due to the surface-photoelectric effect.²⁰ Therefore, we use *p*-polarized 3 ω pulses as probe light. Also, in order to possibly suppress any coherent photoemission processes, we use *s*-polarized 2 ω pump pulses. This cross-polarization combination gives further information on the symmetry of the intermediate states involved in 2PPE.

As seen in the previous section, Si(111) surfaces yield more intense photoemission peaks for energies below the highest-energy peak, compared to Si(001). Also, the low-energy cutoff is smaller than that of Si(001), giving a wider energy window for detecting transient photoemission peaks. Therefore, we conducted the bichromatic 2PPE study mainly on Si(111). The results of time-resolved spectroscopy will be fully described in the next section, and here we summarize additional new features from energy-resolved spectroscopy.

Figure 5(a) shows the bichromatic 2PPE spectra measured by 2 ω and 3 ω laser pulses with $\Delta t = 0$ for $h\nu_0 = 1.65$ and 1.70 eV for Si(111)-(7 × 7). In order to display the spectral components originating from 2PPE processes by 2 ω and 3 ω pulses clearly, we show the difference between the measured spectra at a given Δt and the spectrum measured at $\Delta t = -1$ ps. The spectrum measured at $\Delta t = -1$ ps, where no overlap between two pulses exists, is characterized by simple overlap of the intense one-photon photoemission signal from the surface occupied state S_1 , formed by dangling bonds of adatoms on the 7 × 7 structure, by 3 ω light,^{18,20} and the 2PPE spectrum by the *s*-polarized 2 ω light; the latter is similar to the spectrum shown in Fig. 2(b). We regard the spectrum measured at $\Delta t = -1$ ps as the “background” and subtract it from the measured spectra for $\Delta t > -1$ ps hereafter. The energy axis is the kinetic energy referenced to Φ_V of our samples.

In Fig. 5(a), peak features, consisting of peaks A, B, and Q, similar to those in Fig. 2(a), are evident in the higher-energy region above 1.5 eV. The intense photoemission below 1.5 eV is due to the transiently populated normally unoccupied

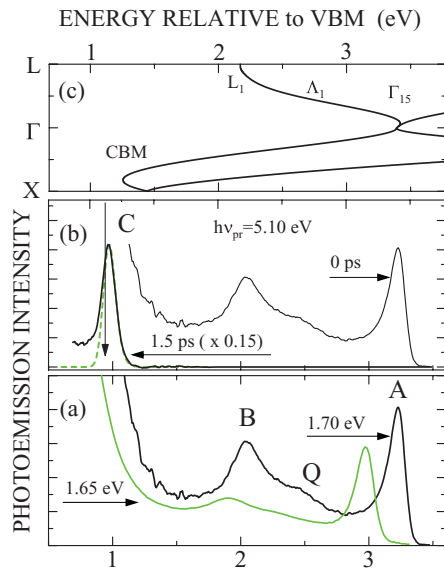


FIG. 5. (Color online) (a) Bichromatic 2PPE spectra of Si(111)-(7 × 7) measured for *s*-polarized 2ω and *p*-polarized 3ω pulses with $\Delta t = 0$ at photon energies of the fundamental wave of 1.65 eV, green (gray) and 1.70 eV, black. Three peaks are labeled as A, B, and Q, similar to the case of Fig. 2. (b) Bichromatic 2PPE spectra measured at time delays for the 3ω probe pulse with respect to the 2ω pump pulse at 0 and 1.5 ps at 293 K. Peak C at 0.97 eV is the photoemission from the CBM (Ref. 20). The green (gray) broken curve is the spectral function of the photoemission from the CBM (see the text). (c) Part of the electronic band structure of Si, showing possible initial states of photoemission probed by 5.10 eV photons. The energy relative to the VBM is calibrated based on the CBM position (vertical arrow in (b)) determined by the peak C in (b), with the band-gap energy of 1.12 eV.

surface state U_1 , formed by dangling bonds of adatoms on the surface.¹⁸ The intensity of peak A is enhanced, relative to that of peak B, compared to the spectrum obtained by monochromatic 2PPE with 2ω pulses. The reason could be due to different properties of final states reached by 2ω and 3ω light and/or possible addition of a coherent photoemission component including intermediate states coupled with 3ω light; there are several possible candidates that act as intermediate states for 3ω light around 5 eV, as can be seen in Fig. 1.

The peak kinetic energies of peaks A and B in Fig. 5(a) are plotted as a function of $h\nu_0$ in Fig. 3(b). Similar to the case of monochromatic 2PPE, E_{KP} is analyzed using the equation: $E_{KP} = m h\nu_0 - E_i$. Peak A gives a value of $m = 5$ with $E_i = 5.34$ eV, while peak B results in a value of $m = 3$ with $E_i = 3.09$ eV. The initial-state energies of peaks A and B are essentially the same as those in the monochromatic 2PPE measurements shown in Fig. 3(a). The value of $m = 5$ for peak A indicates that the coherent 2PPE process by *s*-polarized 2ω and *p*-polarized 3ω pulses is responsible for this photoemission peak. Similarly, the value of $m = 3$ for peak B shows that the initial state of the incoherent two-step process is excited by *s*-polarized 2ω light and ionized by *p*-polarized 3ω light.

For peak A, resonance enhancement of the intensity occurs at 3.40 eV, as shown in the inset of Fig. 2(a), which is close to E'_0 (3.31 ± 0.03 eV). Also, the initial state responsible for peak A is located near the VBM, as analyzed in Table I.

One more important finding for the 2PPE process is that the photoemission can be induced by both *p*-polarized and *s*-polarized light and by orthogonally polarized light, indicating that the intermediate state is a degenerate state. Based on these results, we conclude that peak A of Si(111)-(7 × 7), and peak A' of Si(001) result from coherent 2PPE from the VBM via Γ_{15} . However, we need further investigations on the role of occupied surface states located near the VBM in order to elucidate the photoemission process resulting in peak A. On Si(111)-(7 × 7), the occupied surface state due to rest atoms, S_2 , is located 0.2 eV below the VBM,¹⁹ and on Si(001)-(2 × 1), the occupied dangling-bond band of Si dimers, D_{up} , is located 0.15 eV below the VBM.²¹ Since these occupied surface states form surface resonances with the bulk valence band near the VBM, they may play some role in the photoemission process as well as the VBM.²⁸ We leave the roles of these surface states on the coherent photoemission process generating peak A as an open question for future studies. We simply conclude here that the initial state of peak A is the VBM, since it is clear from energetic analysis in Table I that the VBM is involved in the photoemission process irrespective of a possible role of surface states.

Peak B, which is generated by an incoherent two-step photoemission process, is characterized by the initial state located around 2.1 eV above the VBM. Several band calculations and experiments show that the L_1 state lies 2.29 ± 0.11 eV above the VBM.^{5,29-31} The electronic structure along Λ towards L of the lowest CB is characterized by a dispersionless feature; the energy is almost constant for a range of momenta between $(\pi/a)(0.8, 0.8, 0.8)$ and $(\pi/a)(1, 1, 1)$ (see Fig. 1); all states within this momentum region give essentially the same peak kinetic energy in the photoemission when they are populated. Symmetry considerations tell us that one-photon photoemission normal to the surface from L_1 for *p*-polarized $h\nu_{pr}$ is not possible in the bulk, since dipole transitions cannot connect it to totally symmetric final states.³² On the other hand, Λ_1 , which has almost the same energy as L_1 , can be connected to the totally symmetric final state by *p*-polarized light, which has a field component normal to the surface, but not by the *s*-polarized light. As mentioned in Sec. III A 1, peak B is excited by *p*-polarized light but not by *s*-polarized light in monochromatic 2PPE. As a result of bichromatic 2PPE, peak B is clearly detected by the *s*-polarized 2ω pump pulse and *p*-polarized 3ω probe pulse, showing that the *p*-polarized light is essential for the photoemission process from the transiently populated states. The transient population at the energy of peak B is proven by time-resolved measurement, as will be described in the next section. Therefore, we conclude that peak B is the photoemission from the transiently populated electron states at the region from Λ_1 to L_1 along the Γ - Λ_1 - L_1 line. Peak B' of Si(001)-(2 × 1) may have the same origin, since photoemission near L_1 may become detectable in surface-normal emission by the back folding due to the (2 × 1) reconstruction.

Another important consequence of the 2PPE experiments using 2ω and 3ω pulses is that we can directly correlate our electron kinetic energy to the energy measured from the VBM, free from uncertainties in reported values of ionization energies, since the location of the CBM is clearly defined in the spectra. In Fig. 5(b), we show the spectra measured at

$\Delta t = 1.5$ ps, together with the spectrum at $\Delta t = 0$. In the spectrum at $\Delta t = 1.5$ ps, peaks A, B, and Q have completely been decayed out, and a new peak labeled as C has arisen. Peak C has been attributed to photoemission from the CBM.²⁰ The green (gray) broken curve in Fig. 5(b), which is almost completely overlapped with the 1.5 ps spectrum, is the fitted CBM photoemission spectrum as in Ref. 20. Because of the finite energy resolution of our analyzer, the peak energy of peak C (0.97 eV) is shifted from the exact position of the CBM (0.94 eV) indicated by an arrow. Using the band-gap energy of 1.12 eV at 293 K together with the peak energy (2.05 eV) of peak B, we conclude that the initial state of peak B is located at 2.23 eV above the VBM. Figure 5(c) is a part of Fig. 1, matched to the energy scale based on the result that our kinetic energy of 0.94 eV corresponds to the CBM. The calculated electronic band structure gives us a basis from which we can identify the initial states with real populations probed by 3ω light with $h\nu_{pr} = 5.10$ eV.

In view of Fig. 5, we can make some suggestions on the possible origin of peak Q. Energetically, the initial state of peak Q corresponds to the states near Λ_1 along Γ_{15} to L_1 , when the peak comes from a transient population induced within a pulse-overlap. As seen in Fig. 2, peak Q can be probed only by p -polarized light. Since one-photon photoemission normal to the surface of Si(111)-(7 \times 7) from Λ_1 can be allowed only by p -polarized light, the polarization-dependent result is consistent with this identification. Since the peak kinetic energy does not show any clear shift as a function of $h\nu_0$, as seen in Fig. 3, the photoemission is not from any states with conserving constant energies. When the electrons populated near Λ_1 undergo fast relaxation toward L_1 , a probe-pulse with a finite temporal width of 180 fs may generate a photoemission peak with a kinetic energy determined by a time-dependent average of these relaxing electrons toward low energies. For such relaxing electrons, it might be possible to have almost constant peak kinetic energy of photoemission.

The spectra in Fig. 5(a) show that peak Q is generated even by excitation with photon energy smaller than the resonant energy E'_0 that corresponds to direct transition at Γ . Because of almost parallel dispersions of valence and conduction band along the $\langle 111 \rangle$ direction, many states with finite wave vectors along this direction can contribute to the phonon-assisted indirect transitions for photon energies less than E'_0 .

Since, the photoemission peak Q' of Si(001)-(2 \times 1) shows similar properties as those of peak Q of Si(111)-(7 \times 7), as described in Sec. III A 1, peak Q' of Si(001) may also be attributed to relaxing electrons at states with short lifetimes. Since surface-normal photoemission from the (001) surface can monitor the states along the Γ - Δ -X line of the CB, peak Q' may be due to relaxing electrons temporarily populated at states near Δ_1 . However, detailed future study using shorter optical pulses is needed to elucidate the origin of peak Q (and Q') and to reveal ultrafast scattering processes of highly excited hot electrons within the Γ , L, and X valleys.

B. Time-resolved 2PPE with 2ω and 3ω pulses

Using time-resolved measurements by 2ω pump pulses and 3ω probe pulses, the temporal evolution of photoemission spectra was measured by changing Δt . Figure 6 displays the

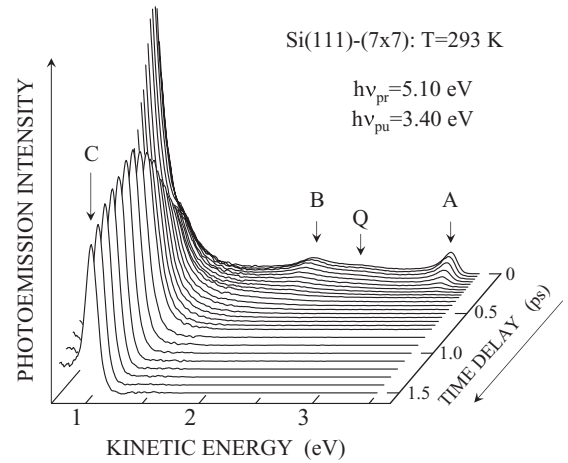


FIG. 6. Series of two-photon photoemission spectra from Si(111)-(7 \times 7) at 293 K for s -polarized, 3.40 eV pump pulses and p -polarized, 5.10 eV probe pulses at Δt 's from 0 to 1.5 ps.

evolution of photoemission spectra upon 3.40 eV excitation, probed with 5.10 eV photons, for time delays up to 1.5 ps after excitation. Analysis of temporal changes of respective peaks gives deeper insight into the relaxation processes of hot electrons generated by 3 eV photons in Si. Characteristic features easily noticed in Fig. 6 are the following. The intensity of peak A at 3.22 eV decays rapidly within 200 fs after excitation. On the other hand, the decay of peak B at 2.05 eV is delayed slightly relative to peak A but takes place within a few hundred femtoseconds of excitation. On the other hand, the CBM peak intensity increases with a significant time delay after excitation. We discuss these features more quantitatively in subsequent sections. Since the efficiencies of detecting photoelectrons emitted from respective positions of the CB may change significantly, we discuss only the relative changes of respective peaks by normalizing the maximum photoemission intensities to unity. We first discuss the L-to-X intervalley scattering in the next section by analyzing the temporal changes of peak B originating from transiently populated electrons near L_1 . Then, we discuss the electron dynamics to form quasi-equilibrated electron systems near the CBM in the subsequent section.

1. L-to-X intervalley scattering

In order to show the temporal evolution of peak B more clearly, we plotted the photoemission intensity I_B of peak B at $E_K = 2.05$ eV, together with that I_A of peak A in Fig. 7(a). The temporal changes were measured also by setting the analyzer at a fixed electron energy with scanning Δt . The time-scan data are shown by open circles, while the intensities determined from the spectra of Fig. 6 are shown by solid circles. As concluded previously herein, peak A is due to a coherent 2PPE process, and the change of its intensity with respect to Δt can be regarded as the cross-correlation trace (CCT) of our pump and probe pulses. The intensity I_A , shown by the red (dark-gray) curve, shows almost complete symmetric shape with respect to $\Delta t = 0$, and can be fitted by a Gaussian distribution with full-width at half maximum of 210 fs. On the other hand, I_B shows a finite delay of the peak around $\Delta t = 0$ ps

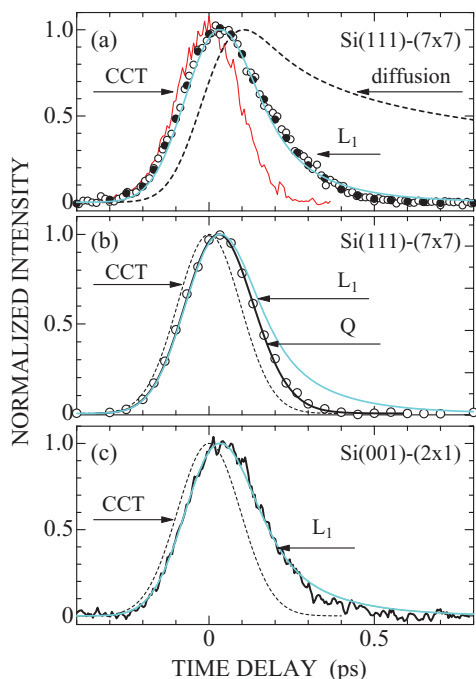


FIG. 7. (Color online) (a) Temporal changes of population n_L near L_1 determined from the photoemission intensity of peak B, open and solid circles, and the cross-correlation trace, CCT, between pump and probe pulses, red (dark gray) curve. The broken curve shows the calculated electron density at the surface region as a function of time delay using a diffusion equation model without any other decay channels. The light blue (gray) curve data points are the simulated result of the diffusion equation model with a single decay channel characterized by a time constant $\tau_L = 180$ fs. (b) Temporal change of the intensity of peak Q, open circles, compared with the cross-correlation trace, broken curve, and decay of the population near L_1 , light blue (gray) curve. (c) Temporal changes of the intensity of peak B' of Si(001)-(2 × 1), compared with the cross-correlation trace, broken curve, and decay of the population near L_1 , light blue (gray) curve, obtained for peak B of Si(111)-(7 × 7).

and a persistent decay; an ~ 150 fs time constant is estimated at $\Delta t > 200$ fs, where pump and probe pulses no longer overlap. The delay of the peak maximum with respect to the peak of CCT demonstrates clearly that the peak is associated with a real population. Therefore, we can definitively conclude that peak B is due to photoemission from transiently populated electrons near L_1 . Since the momentum scattering time to dephase excited-carrier states is shorter (~ 30 fs³³) than our pump- and probe-pulse widths, photoemission from the temporally occupied states by the pump pulse can be detected even in the spectrum at $\Delta t = 0$ ps, as well as by monochromatic 2PPE using 2ω pulses as displayed in Fig. 2(a).

In Fig. 7(b), we plot the photoemission intensity of peak Q, based on the time-resolved spectra in Fig. 6. The temporal change is compared with the CCT and the L_1 peak. The intensity of peak Q shows a finite delay with respect to the CCT, but it decays faster than the L_1 peak. The result shows that peak Q is due to the photoemission from transiently populated electrons at states that have short lifetimes, supporting our tentative conclusion that peak Q is due to relaxing electrons at the state near Λ_1 along Γ_{15} to L_1 .

For quantitative analysis of the ultrafast changes in CB-electron populations under excitation above 3 eV, it is crucial to take the effect of diffusion into account, since the large absorption coefficient ($> 10^6$ cm⁻¹, Ref. 14) results in a steep carrier concentration gradient that leads to efficient carrier diffusion. Since 2PPE probes the electron dynamics only near the surface region, efficient diffusion can significantly reduce photoemission intensities. To demonstrate the effects of diffusion, we display in Fig. 7(a) the simulated result for the CB electron density at the surface, calculated by a diffusion-equation model with an equilibrated ambipolar diffusion constant $D (= 18$ cm²s⁻¹) at 300 K.³⁴ No other decay channels are included in the calculation. The initial density at the surface is reduced to roughly one half within 1 ps of excitation, during which several relaxation processes may take place. The intensity I_B of peak B in Fig. 7(a) shows a faster decay than the diffusion-equation result. Then, we analyzed the temporal evolution of the population n_L near L_1 using the diffusion equation including a single decay channel characterized by a time constant τ_L , as

$$\frac{\partial n_L(t, z)}{\partial t} = G(t, z) - D \frac{\partial^2 n_L(t, z)}{\partial z^2} - \frac{1}{\tau_L} n_L(t, z), \quad (1)$$

where z is the distance from the surface toward bulk, and $G(t, z)$ is the carrier generation rate determined by a pump-laser pulse shape and the absorption coefficient. By solving the equation, we obtained temporally and spatially resolved $n_L(t, z)$. To compare the simulation results with experimentally determined values, we assumed that I_B is proportional to n_L at $z = 0$, since photoemission probes only those in the surface region. The best fit is obtained for $\tau_L = 180 \pm 20$ fs.

It is still unresolved how to best characterize the dynamical transport properties of hot electrons in short temporal domains. In order to examine the incorporation of several possible dynamical effects, like ballistic transport of hot electrons, into our present diffusion-equation model, we performed simulations using several fixed values of the diffusion constant D between 10 and 50 cm²s⁻¹. Temporal change of I_B was rather insensitive to the magnitude of D , and the best-fit procedure always gives $\tau_L = 180 \pm 20$ fs. Therefore, we conclude that electrons near L_1 decay with a 180 fs time constant.

The decay of the electron population near L_1 may be governed either by scattering to the X valley and/or surface recombination into the unoccupied surface states. In order to examine possible effects of surface recombination, we conducted similar studies for Si(001)-(2 × 1), which has completely different surface electronic states than Si(111)-(7 × 7).¹⁹ As shown in Fig. 4, the population near L_1 can be probed by measuring the intensity of peak B' of Si(001)-(2 × 1). The temporal changes in the L_1 peak intensity of Si(001)-(2 × 1) are shown in Fig. 7(c). The intensity decays within 500 fs after excitation while showing a finite delay with respect to the CCT shown by the broken curve. The analysis, similar to that for Si(111)-(7 × 7) in terms of the diffusion-equation model, shows that the lifetime of the L_1 peak is 175 ± 30 fs for Si(001)-(2 × 1), which is essentially the same value as for τ_L in Si(111)-(7 × 7). The light blue (gray) curve pertaining to data points is the same one used for I_B of Si(111)-(7 × 7) in Fig. 7(a). This result shows that τ_L is

not surface sensitive, and that the scattering into the X valley in the bulk electronic state is the primary relaxation process of electrons populated near L₁ in Si.

We also studied the effects of sample temperature T and excitation density ρ_e on τ_L . We find that τ_L is not dependent on ρ_e for electron densities ranging from 3×10^{17} to $5 \times 10^{18} \text{ cm}^{-3}$, but it is dependent on T ; the lifetime at 90 K is 250 fs, which is about 40% longer than at 293 K. These results substantiate the dominant role of electron-phonon interaction on intervalley scattering for $\rho_e < 5 \times 10^{18} \text{ cm}^{-3}$.

In a homopolar semiconductor such as Si, L-X intervalley scattering occurs by the deformation potential interaction. The transition rate, R , is given by³⁵

$$R(k) = (\pi D_{LX}^2 / \rho_m \omega_{LX}) \{2n_{BE}(\omega_{LX}) + 1\} N(E_k - \Delta E_{LX}), \quad (2)$$

where D_{LX} is the deformation potential constant, ρ_m is the mass density, ω_{LX} is the angular frequency of the phonon mode responsible for the scattering, E_k is the energy of the initial state relative to L₁, ΔE_{LX} is the difference in energy of the two valley minima, and $N(E_k - \Delta E_{LX})$ is the final density of states of the CB to which the electron scatters. The term $n_{BE}(\omega_{LX})$ is the Bose-Einstein occupation probability of phonons with the frequency ω_{LX} . In Eq. (2), we assumed that the phonon energy $\hbar\omega_{LX}$ is much smaller than the magnitude of ΔE_{LX} . In Fig. 8, we show an iso-energy plane of the lowest CB in the Brillouin zone including L₁. From the figure, we can estimate that the smallest phonon momentum that can induce L-to-X intervalley scattering corresponds to the wave vector of 0.63 \AA^{-1} . The direction is almost parallel to the direction from K to Γ . The phonon dispersion in Si³⁶ tells that the LA phonon with this momentum has an energy quantum of 29.8 meV. This magnitude of phonon energy well describes quantitatively the temperature-dependent changes in τ_L described previously via the factor $\{2n_{BE}(\omega_{LX}) + 1\}$ in Eq. (2). Therefore, we interpret that this LA phonon is responsible for the intervalley scattering; $\omega_{LX} = 4.4 \times 10^{13} \text{ s}^{-1}$.

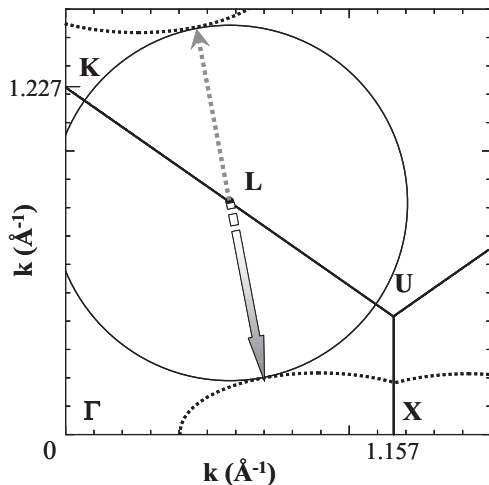


FIG. 8. Two-dimensional plot of iso-energy states, broken curve, with L₁ in the lowest CB in the Brillouin zone of Si. The minimal phonon momentum required by a one-phonon-emission process of L-to-X intervalley scattering is estimated to be 0.63 \AA^{-1} .

Because $\Delta E_{LX} > \hbar\omega_{LX}$, we assume $N(E_k - \Delta E_{ij} - \hbar\omega_{LX}) \approx N(E_k - \Delta E_{ij} + \hbar\omega_{LX})$, resulting in Eq. (2). We also presume that quasithermalization of hot carriers in the L valley takes place within 100 fs due to effective carrier-carrier interaction in a valley, as in the case of III-V semiconductors,¹⁵ and assume for simplicity that $E_k = 0$. The term $N(E_k - \Delta E_{LX})$ was estimated using the density of state effective mass of $0.33m_0$ (m_0 is the electron rest mass) without anharmonic corrections. Then, for $D_{LX} = 1.2 \text{ eV\AA}^{-1}$, together with other well-established values for Si, we calculate a rate of $5.6 \times 10^{12} \text{ s}^{-1}$, which corresponds to a lifetime of 180 fs at 293 K.

Previous studies on intervalley scattering among six degenerate ellipsoidal energy minima of the CB determined two deformation potential constants; $D_f = 6.85 \text{ eV\AA}^{-1}$ for the f -scattering process and $D_g = 0.6\text{--}0.7 \text{ eV\AA}^{-1}$ for the g -scattering process.³⁷ The value for L-to-X intervalley scattering is close to that of D_g , but it is much smaller than for polar semiconductors like GaAs and InP, which have been studied extensively.¹⁵

2. Relaxation of hot electrons toward the CBM

Figure 6 also shows that the CBM peak intensity reaches its maximum with a significant time delay about 1 ps after excitation. This is substantially longer than that for excitation below 2.2 eV, which results in the electron injection into the X valley as observed in the previous study¹³ Here, we discuss the hot-electron relaxation leading to the accumulation near the CBM to elucidate the feature of delayed accumulation of electrons near the CBM.

First, we evaluate the density, n_C , of electrons accumulated near the CBM when excited by 3.40 eV photons, based on the results shown in Fig. 6. The density cannot be simply estimated by the peak intensity of the photoemission peak only, since the spectral shape changes substantially depending on the effective temperature of the electronic system.¹³ In order to evaluate n_C , we employed spectral shape analysis in terms of the electron distribution function $f(e)$. Since ρ_e is still lower than the effective density-of-state of the CB, we can use the Boltzmann distribution function to describe the electron statistics.¹³ Therefore, $f(e)$ is given by

$$f(e) = \frac{2I}{\sqrt{\pi}(k_B T^*)^{3/2}} \sqrt{e} \exp\left(-\frac{e}{k_B T^*}\right), \quad (3)$$

where I is a constant that characterizes the density, k_B is the Boltzmann constant, T^* is the effective temperature, and e is the energy measured from the CBM. We fit the observed emission spectra with spectral function $F(e)$, which is the $f(e)$ convolved with the energy resolution ΔE of detection.³⁹ The density of electrons near the CBM is obtained as a function of Δt by integrating the time-resolved spectral function $F(e)$ over energy.

In Fig. 9, we show typical examples of the results of the analysis. Because of the considerable overlap of the CBM peak with the U₁ component of the surface states in the relevant kinetic energy region, it is essential to separate the two components reasonably. As shown in Fig. 9(a), when Δt is negative, where the electron density near the CBM is expected to be minimal, the photoemission spectrum in the energy range is a smoothly decreasing function. The spectrum

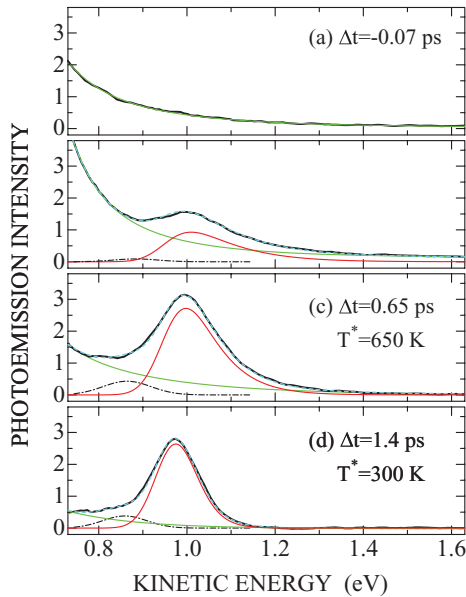


FIG. 9. (Color online) Spectral deconvolution of pump-induced photoemission spectra (thick solid curves) of Si(111)-(7 × 7) into the component originating from the surface unoccupied state U_1 , green (gray) curve, and the peak from the CBM, red (dark gray), at time delay of -0.07 ps (a), 0.2 ps (b), 0.65 ps (c), and 1.4 ps (d). The chain curves show the estimated peak from defect states (see Ref. 40). The broken light blue (gray) curve is the fit obtained by the analysis.

can be fitted well by a *base function* consisting of the sum of two exponential functions and a constant, as shown by the green (gray) curve. We use this base function to approximate the U_1 component, which shows a rather steep decrease in the lower-energy range and gradual decrease in the higher-energy range. In the spectra at positive time delays, the photoemission peak from the CBM is clearly visible, and the spectra are fitted as the sum of the base function and the spectral function $F(e)$. The red (dark gray) curve in each column in the figure is the spectral function of the CBM photoemission thus resolved, and each is characterized by the effective temperature listed.⁴⁰

In this spectral analysis, including several parameters, some ambiguities are unavoidable to evaluate n_C . However, the obtained results are rather robust; the description of the U_1 component by a polynomial, or the linear extrapolation between 0.8 and 1.2 eV give essentially the same results, with variations less than 10% when normalized to the maximum value. The density of electrons near the CBM, obtained by integrating the time-resolved distribution function, is shown in Fig. 10(a). The population n_C reaches a peak value at 660 fs after excitation and then decays substantially within 2 ps. The decay may be due to efficient diffusion toward the bulk and/or transfer to unoccupied surface states. The effective temperature obtained by the analysis is plotted in Fig. 10(c).

When we compare the growth of the CBM density n_C and the decay of population n_L near L_1 , we find a substantial delay between the two; there is a finite time lag between the decay of n_L and the growth of n_C . Since there is a large energy difference of 1.1 eV between L_1 and the CBM as determined in Sec. III A 2, we presume that the lag reflects relaxation down to the CBM in the X valley after scattering from the L

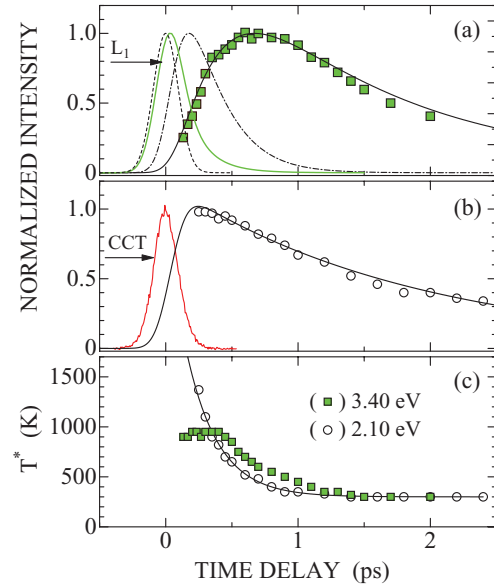


FIG. 10. (Color online) (a) Temporal evolution of electron density accumulated near the CBM upon 3.40 eV excitation. The growth curve is compared with the CCT, broken curve, the temporal change of L_1 peak, green (gray) curve, and estimated temporal changes of relaxing electrons, chain curve. The solid curve is the best-fit curve of the diffusion equation model (see text). (b) Temporal evolution of electron density accumulated near the CBM upon 2.10 eV excitation. The cross-correlation trace, red (dark-gray) curve, was characterized by the full-width at half maximum of 205 fs. (c) Evaluated effective temperature of quasi-equilibrated electron distributions near the CBM for the case of 3.40 eV excitation, square, and of 2.10 eV excitation, open circle.

valley. As suggested in Sec. III A 2, a certain fraction of hot electrons may be scattered into the X valley, without being scattered into the L valley. Since the photoemission peak of Q' of Si(001)-(2 × 1) has a peak energy about 0.5 eV higher than peak B' from L_1 , the energy difference from the CBM can be estimated to be about 1.4 eV. Such hot electrons are also expected to relax down toward the CBM with a finite relaxation time.

Based on the presumption mentioned previously, we analyze the growth kinetics of electron accumulation near the CBM using a diffusion equation model to characterize the delay in accumulation more quantitatively. For simplicity of the analysis, we neglected the contribution of hot electrons scattered directly into the X valley. Temporal evolutions of n_L , n_C , and the population n_R of the relaxing electrons can be correlated by the following set of diffusion equations;

$$\frac{\partial n_R(t, z)}{\partial t} = \frac{1}{\tau_L} n_L(t, z) - D \frac{\partial^2 n_R(t, z)}{\partial z^2} - \frac{1}{\tau_R} n_R(t, z), \quad (4)$$

$$\frac{\partial n_C(t, z)}{\partial t} = \frac{1}{\tau_R} n_R(t, z) - D \frac{\partial^2 n_C(t, z)}{\partial z^2} - \frac{1}{\tau_C} n_C(t, z), \quad (5)$$

together with the equation for n_L (Eq. (1)). The same value of D ($=18$ cm²s⁻¹) was assumed for n_L , n_R , and n_C , for simplicity. Since photoemission probes only the populations in the surface region, we assumed that photoemission intensities of respective states are proportional to the values at $z = 0$ of temporally and spatially resolved $n_R(t, z)$, and $n_C(t, z)$. The

green (gray), chain, and solid curves in Fig. 10(a) are the simulated results of the set of diffusion equations. By inserting the relaxing-electron state, the time lag for forming the electron population near the CBM is reasonably described. The best-fit values for τ_R and τ_C are 150 fs and 2.0 ps, respectively. From the results of the analysis, we may conclude that the electrons scattered into the X valley from L valley are accumulated near the CBM with a finite time delay characterized by τ_R of 150 fs.

We compare the temporal evolution of CBM electron density populated by 3.40 eV photons with that induced by electron injection directly into the X valley by photoexcitation with 2.10 eV photons. In order to see the changes specific to the excitation photon energy, the Si(111)-(7 × 7) surface, used in time-resolved 2PPE with 3.40 eV photons, was specifically used in the measurements, since the electrons near the CBM for Si(001)-(2 × 1) apparently show a different decay characteristic from that for Si(111)-(7 × 7).¹³ Similar spectral analysis was applied to evaluate the electron density near the CBM as a function of Δt with respect to the 2.10 eV pump pulse, and the results are plotted in Fig. 10(b). In the case of 2.10 eV excitation, however, there is a significant overlap of the CBM peak and a broad coherent 2PPE peak in the relevant kinetic energy region.¹³ Therefore, it was not possible to evaluate accurately the density for Δt 's less than 200 fs. Nevertheless, it is clear that the electron density reaches a maximum at 200 fs and decays gradually within the time window of detection. The solid curve data points are a calculated result of a rate-equation model with formation time of 40 fs and decay time of 1.8 ps¹³; no effects of diffusion can be expected for the 2.10 eV excitation because of the small absorption coefficient. Since the decay rate of the CBM density is similar to that by 3.40 eV excitation, the difference in the population kinetics seen in Figs. 10(a) and 10(b) directly reflects the growth rate. Therefore, by comparison, it is evident that there exists a substantial delay in electron accumulation near the CBM when they are excited by photon energies of more than 3 eV.

In the relaxation processes of hot electrons with excess energies, relative to the CBM, exceeding the band gap energy, excitation of electron-hole pairs can be a possible decay channel as in metals.⁴¹ If this channel takes place with a rate higher than phonon-assisted relaxation, then we expect fast generation of electrons just near the CBM. However, as demonstrated here, accumulation of electrons near the CBM is delayed substantially compared to the case of electrons injected directly into the X valley by photons with energies below 2.2 eV. Therefore, the present result shows that the excitation of electron-hole pairs is not a dominant channel in the relaxation of highly excited hot electrons in Si.

The effective electron temperature T^* , obtained by the spectroscopic analysis, is shown in Fig. 10(c) for the two cases of 2.10 eV excitation and 3.40 eV excitation. For 2.10 eV excitation, T^* is 1350 K at $\Delta t = 250$ fs, and it decreases exponentially toward ambient temperature. The decrease of T^* is characterized by a time constant of 240 fs, which has been interpreted as the energy relaxation time.¹³ On the other hand, in the case of 3.40 eV excitation, T^* is 950 K, which is almost constant before forming the maximum electron population near the CBM, and which decreases toward ambient temperature within 2 ps of excitation. The decrease could be

fitted by an exponential decay with a time constant of 440 fs. This value is larger than the energy relaxation time of 240 fs determined for excitation-photon energies less than 2.2 eV. It is known that the energy relaxation time of hot electrons in semiconductors may change, depending on the density of excitation due to plasma-induced screening.⁴² However, the maximum density of carriers in the present study is at most $1 \times 10^{19} \text{ cm}^{-3}$, i.e., far below the critical density of $1 \times 10^{21} \text{ cm}^{-3}$.⁴²⁻⁴⁴ Therefore, this screening effect plays no role in the present study, and the slower time constant is a consequence of relaxation of hot electrons generated by 3.40 eV photons.

Relaxation processes of optically injected hot electrons with nonequilibrium distributions toward quasi-equilibrated electronic systems near the CBM may be governed by the interplay between electron-phonon interaction and carrier-carrier interaction. The former interaction transfers the excess electronic energy to the lattice, while the carrier-carrier interaction leads to a quasi-equilibrated electron distribution maintaining the internal electronic energy. Therefore, the magnitude of T^* and its temporal change are dependent on several factors, like the amount of excess energy each electron carries, mode of hot-electron supply, and the rate of dissipation of internal energy. Efficient carrier diffusion may also play a role in the cooling process of hot electrons in the surface region.

As seen in Fig. 10(a), there is a significant time delay in the accumulation of electrons near the CBM in the case of 3.40 eV excitation. The delay comes from several relaxation processes, including intervalley scattering and energy relaxation in the X valley from states more than 1 eV above the VBM, as analyzed herein. These processes transfer the excess electronic energy to the lattice, and modify the mode of hot-electron supply into the vicinity of CBM from the Gaussian-like form determined by the short pump-pulse to a stochastic form characterized by a relaxation time of a few hundreds of femtoseconds. Therefore, it may be expected that the magnitude and temporal change of T^* of the finally formed quasi-equilibrated electron system are dependent on the excitation photon energy, which results in different relaxation pathways. The average energy $3/2k_B T^*$ of quasi-equilibrated electrons near the CBM is at most 0.1 eV for $T^* = 950$ K, which is much smaller than the electron excess energy (1.14 eV) defined by a half of $h\nu_{\text{pump}} - E_g$.¹³ Therefore, most of the internal energy of electrons given by photoexcitation is transferred to the lattice before establishing the quasi-equilibrated electronic distribution. This may be one important characteristic of relaxation of highly excited hot electrons excited with 3 eV photons in Si.

IV. SUMMARY

We present a 2PPE study of the dynamical relaxation of highly excited hot electrons in Si for excitation-photon energies ranging from 3.2 to 3.5 eV. Monochromatic 2PPE reveals a coherent 2PPE peak from the VBM, and a transient photoemission peak from L₁ region. Time-resolved 2PPE measurements show that electrons injected into L valley undergo the L-to-X intervalley scattering with a time constant of 180 fs (250 fs) at 293 (90) K. For the scattering, a deformation potential constant of 1.2 eV \AA^{-1} is obtained. The highly excited electrons relax down toward the CBM

to form a quasi-equilibrated hot electron distribution; the highest density is accumulated at 660 fs after excitation. The hot electron distribution is equilibrated with the lattice within 2 ps after excitation. These features of hot-electron relaxation, significantly different from those for excitation below 2.2 eV, demonstrate relaxation pathways dependent on the excitation photon energy. The results obtained in this study may provide a sound foundation on which we can investigate

in detail structural rearrangement phenomena induced by photoexcitation near 3 eV in Si.

ACKNOWLEDGMENTS

This work was supported by a Specially Promoted Research of Grant-in-Aid for Scientific Research from the Ministry of Education, Science, Technology, Sports, and Culture of Japan.

*tanimura@sanken.osaka-u.ac.jp

¹B. Fischer and K. R. Hofmann, *Appl. Phys. Lett.* **76**, 583 (2000).

²M. Hase, M. Kitajima, A. M. Constantinescu, and H. Petek, *Nature* **426**, 51 (2003).

³J. Kanasaki and K. Tanimura, *Phys. Rev. B* **66**, 125320 (2002).

⁴M. Harb, R. Ernstorfer, C. T. Hebeisen, G. Sciaini, W. Peng, T. Dartigalongue, M. A. Eriksson, M. G. Lagally, S. G. Kruglik, and R. J. Dwayne Miller, *Phys. Rev. Lett.* **100**, 155504 (2008).

⁵M. Rohlfing, P. Krüger, and J. Pollmann, *Phys. Rev. B* **52**, 1905 (1995); M. Rohlfing (private communication).

⁶M. Cardona, K. L. Shaklee, and F. H. Pollak, *Phys. Rev.* **154**, 696 (1967).

⁷J. W. Grovwe and P. Handler, *Phys. Rev. B* **9**, 2600 (1974).

⁸K. Kondo and A. Moritani, *Phys. Rev. B* **14**, 1577 (1976).

⁹G. Jungk, *Phys. Status Solidi B* **99**, 643 (1980).

¹⁰A. Daunois and D. E. Aspnes, *Phys. Rev. B* **18**, 1824 (1978).

¹¹P. Lautenschlager, M. Garriga, L. Vina, and M. Cardona, *Phys. Rev. B* **36**, 4821 (1987).

¹²S. Tsoi, R. Rodriguez, A. K. Ramdas, J. W. Ager III, H. Riemann, and E. E. Haller, *Phys. Rev. B* **72**, 153203 (2005).

¹³T. Ichibayashi and K. Tanimura, *Phys. Rev. Lett.* **102**, 087403 (2009).

¹⁴D. E. Aspnes and A. A. Studna, *Phys. Rev. B* **27**, 985 (1983).

¹⁵L. Rota, P. Lugli, T. Elsaesser, and J. Shah, *Phys. Rev. B* **47**, 4226 (1993).

¹⁶R. Haight, *Surf. Sci. Rep.* **21**, 275 (1995).

¹⁷J. E. Demuth, W. J. Thompson, N. J. DiNardo, and R. Imbihl, *Phys. Rev. Lett.* **56**, 1408 (1986).

¹⁸M. Mauerer, I. L. Shumay, W. Berthold, and U. Höfer, *Phys. Rev. B* **73**, 245305 (2006).

¹⁹W. Mönch, *Semiconductor Surfaces and Interfaces* (Springer, Berlin, 1995).

²⁰T. Ichibayashi and K. Tanimura, *Phys. Rev. B* **75**, 235327 (2007).

²¹C. Kentsch, M. Kutschera, M. Weinelt, Th. Fauster, and M. Rohlfing, *Phys. Rev. B* **65**, 035323 (2001).

²²G. Hollinger and F. J. Himpsel, *J. Vac. Sci. Technol. A* **1**, 640 (1983).

²³C. Sebenne, D. Bolmont, G. Guichar, and M. Balkanski, *Phys. Rev. B* **12**, 3280 (1975).

²⁴K. Tanimura and J. Kanasaki (unpublished).

²⁵K. I. Shudo, S. Takeda, and T. Munakata, *Phys. Rev. B* **65**, 075302 (2002).

²⁶I. Andriamanantenaso, J. P. Lacharme, and C. A. Sébenne, *J. Vac. Sci. Technol. A* **5**, 902 (1987).

²⁷J. P. Lacharme, N. Benazzi, and C. A. Sébenne, *Surf. Sci.* **433-435**, 415 (1999).

²⁸C. Eickhoff, M. Teichmann, and M. Weinelt, *Phys. Rev. Lett.* **107**, 176804 (2011).

²⁹D. Straub, L. Ley, and F. J. Himpsel, *Phys. Rev. Lett.* **54**, 142 (1985).

³⁰Y. Lassailly, P. Chiaradia, C. Hermann, and G. Lampel, *Phys. Rev. B* **41**, 1266 (1990).

³¹J. E. Ortega and F. J. Himpsel, *Phys. Rev. B* **47**, 2130 (1993).

³²W. Eberhardt and F. J. Himpsel, *Phys. Rev. B* **21**, 5572 (1980).

³³A. J. Sabbah and D. M. Riffe, *Phys. Rev. B* **66**, 165217 (2002).

³⁴H. M. van Driel, *Phys. Rev. B* **35**, 8166 (1987).

³⁵B. K. Ridley, *Quantum Processes in Semiconductors* (Oxford University Press, Oxford, 1988).

³⁶W. Weber, *Phys. Rev. B* **15**, 4789 (1977).

³⁷J. G. Nash and J. W. Holm-Kennedy, *Phys. Rev. B* **15**, 3994 (1977).

³⁸A. Rettenberger and R. Haight, *Surf. Sci.* **414**, 197 (1998).

³⁹The instrumental energy resolution of our detector is typically 50 meV. However, a finite energy spread of probe pulse cannot be ignored in the time-resolved 2PPE experiments. Also, space-charge effects due to a huge number of low-kinetic energies emitted from a one-photon process from S_1 may possibly broaden the energy resolution. In this analysis, we used $\Delta E = 80$ meV, which was adopted by fitting the CBM photoemission peaks measured at Δt 's larger than 1.5 ps. See the example in Fig. 5(b).

⁴⁰In the spectra measured at longer time delays, introduction of gap-state peaks shown by thin solid curves in Figs. 9(c) and 9(d) makes the fitting almost perfect. Although our Si(111)-(7 × 7) surfaces have excellent qualities, a finite amount of defects are still unavoidable. These defects may contribute to photoemission at energy region below the band gap. However, the contribution is not very significant, and we can neglect its effect in the fitting by putting more weight into the energy region larger than the band-gap energy.

⁴¹P. M. Echenique, J. M. Pitarke, E. V. Chulkov, and A. Rubio, *Chem. Phys.* **251**, 1 (2000).

⁴²E. J. Yoffa, *Phys. Rev. B* **21**, 2415 (1980); **23**, 1909 (1981).

⁴³T. Sjodin, H. Petek, and H.-L. Dai, *Phys. Rev. Lett.* **81** 5664 (1998).

⁴⁴M. Harb, R. Ernstorfer, T. Dartigalongue, C. T. Hebeisen, R. E. Jordan, and R. J. Dwayne Miller, *J. Phys. Chem. B* **110**, 25308 (2006).